

# Nanocrystalline indium oxide-doped tin oxide thin film as low temperature hydrogen sensor

S. Shukla<sup>a</sup>, S. Seal<sup>a,\*</sup>, L. Ludwig<sup>b</sup>, C. Parish<sup>b</sup>

<sup>a</sup> *Department of Mechanical Materials Aerospace Engineering (MMAE) and Advanced Materials Processing and Analysis Center (AMPAC), Engineering # 381, 4000 Central Florida Blvd., University of Central Florida (UCF), Orlando, FL 32816, USA*

<sup>b</sup> *Kennedy Space Center (KSC), NASA, Titusville, FL, USA*

Received 7 May 2003; received in revised form 21 August 2003; accepted 28 August 2003

## Abstract

Hydrogen gas, within the concentration range of 100 ppm–4 vol.%, is successfully sensed at lower operating temperatures, 25 and 50 °C, using the Pt-sputtered sol–gel dip-coated nanocrystalline (6–7 nm) 6.5 mol% In<sub>2</sub>O<sub>3</sub>-doped SnO<sub>2</sub> semiconductor thin (100–150 nm) film sensor. Typically, for 1000 ppm of hydrogen, the maximum sensitivity values of 32 and 1600% are observed at 25 and 50 °C, respectively; while for 2 vol.% hydrogen, the maximum sensitivity values of 50 and 70,000% are recorded at 25 and 50 °C, respectively. At 25 °C, for 4 vol.% (explosive limit as set by NASA) hydrogen, the maximum hydrogen gas sensitivity values of 107,887 and 2083% are observed for the Pt-sputtered thin films calcined at 500 and 600 °C, respectively.

© 2003 Elsevier B.V. All rights reserved.

**Keywords:** Nanocrystalline indium oxide-doped tin oxide; Pt-sputtered thin film; Low temperature hydrogen sensor

## 1. Introduction

In recent years, research interest in hydrogen as a near-future fuel has increased because it is renewable, abundant, efficient, and unlike other alternatives, provides zero emissions. The product of hydrogen combustion is water, making it the most environmentally friendly fuel. Hydrogen can be used either as a fuel for direct combustion or as a fuel for fuel cells, which in turn, generate direct current electricity to power an electric motor. The amount of energy produced by hydrogen, per unit weight of fuel, is about three times the energy contained in an equal weight of gasoline and nearly seven times that of coal. The public transport fueled by hydrogen is, hence, very likely in near future.

On the other hand, in the US space program, hydrogen is used by NASA primarily to launch the space vehicles. NASA has used liquid hydrogen for the last three decades to propel the space shuttle and other rockets into orbit. Hydrogen fuel cells power the shuttle's electrical systems, producing a clean byproduct (pure water), which the crew drinks.

Hence, it is envisaged that hydrogen will form the basic energy infrastructure that will power future societies.

However, if handled carelessly, hydrogen is as dangerous for transport, storage, and use as many other fuels. As a result, safety remains a top priority in all the aspects of hydrogen energy, and as a result, sensing the hydrogen leakage from the storage and the transportation equipment, which are mostly utilized at room temperature, has become very essential. Although different types of sensors, based on different principles are currently investigated [1–9], most of them pose problems in sensing very low hydrogen concentrations with very high efficiency at lower operating temperatures (<200 °C). Much focused work is, therefore, needed in the development of novel sensor materials with very high sensitivity and selectivity towards hydrogen, specifically close to room temperature.

On the other hand, in recent years, nanotechnology has emerged as an attractive field for the development of novel materials having unusual properties and has provided different pathways to solve many unresolved issues in various fields. As a result, nanocrystalline SnO<sub>2</sub> semiconductor gas sensors, based on resistance-change mechanism have been extensively investigated for hydrogen detection [10–32]. However, in general, there are several major issues associated with them, which are not yet completely resolved, and hence, need further attention.

\* Corresponding author. Tel.: +1-407-823-5277; fax: +1-407-823-0208.  
E-mail address: [sseal@pegasus.cc.ucf.edu](mailto:sseal@pegasus.cc.ucf.edu) (S. Seal).

First, the maximum gas sensitivity of nanocrystalline semiconductor SnO<sub>2</sub> sensor lies well-above room temperature (350–400 °C). Secondly, the nanocrystalline SnO<sub>2</sub> thin film gas sensors exhibit enhanced sensitivity below 10 nm crystallite size [33]; however, they tend to show an increased response time with decreasing nanocrystallite size below this size range [33,34]. Third, the existing gas sensing mechanism [35], proposed for explaining the gas sensitivity enhancement below 10 nm crystallite size, can not satisfactorily explain the increased response time below this size range. Hence, the mechanism of gas sensing using semiconductor oxide sensors is not yet completely understood. Fourth, the response and the recovery time have also been observed to increase drastically at lower operating temperatures (<200 °C). Fifth, not a single sensor material, based on any mechanism and synthesis approach have been developed, which would be highly selective to all reducing gases. Sixth, since the semiconductor oxide sensors exhibit enhanced gas sensitivity when they are synthesized in the nanocrystalline form, they pose a major problem when they are operated at higher temperatures. New ways must be developed to restrict the growth of the nanocrystalline grains at higher temperatures to expand their operating temperature range.

Hence, knowing the importance of hydrogen and the issues associated with the semiconductor oxide gas sensors, attempt is made in this investigation, to resolve at least one of the major issues discussed above. The primary goal of the present article is, hence, set to detect hydrogen, using the sol–gel derived nanocrystalline-doped SnO<sub>2</sub> semiconductor oxide thin film sensor, at lower operating temperatures (room temperature (25 °C) and 50 °C).

## 2. Experimental

### 2.1. Materials

Tin(IV)-isopropoxide (Sn[OC<sub>3</sub>H<sub>7</sub>]<sub>4</sub>) (10%, w/v) in isopropanol (72 vol.%) and toluene (18 vol.%) and indium(III)-isopropoxide (In[OC<sub>3</sub>H<sub>7</sub>]<sub>3</sub>) were purchased from Alfa Aesar (USA) and used as received. Small glass substrates (1 cm × 1 cm) were cut from the Pyrex glass slides, which were received from the Fisher Scientific (USA), for the dip-coating experiments.

### 2.2. Processing of nanocrystalline indium oxide (In<sub>2</sub>O<sub>3</sub>)-doped tin oxide (SnO<sub>2</sub>) thin films

Pure SnO<sub>2</sub> and indium oxide (In<sub>2</sub>O<sub>3</sub>)-doped SnO<sub>2</sub> thin films coated on the Pyrex glass (silica) substrates were processed via sol–gel dip-coating technique. The glass substrates were ultrasonically cleaned, first in acetone and then in isopropanol. For synthesizing pure SnO<sub>2</sub> thin films, the pre-cleaned substrates were dipped in the solution of tin-isopropoxide in isopropanol and toluene, corresponding

to the concentration of 0.23 M of tin-isopropoxide, using a dip-coater with a withdrawal speed of 150 cm/min. For synthesizing doped SnO<sub>2</sub> thin films, calculated amount of indium(III)-isopropoxide was dissolved in this solution to obtain the thin films of SnO<sub>2</sub>–6.5 mol% In<sub>2</sub>O<sub>3</sub>. After the dip-coating process, the gel films were dried at 150 °C for 1 h in air. The substrates were dip-coated again using the respective solutions under similar conditions and then dried again at 150 °C for 1 h in air. Some of the dried gel films were sputtered with a thin (3–5 nm) layer of Pt for 10 s using a sputter coater (K350, Emitech Ltd., Ashford, Kent, England). Finally, Pt-sputtered and non-Pt-sputtered dried films were fired at 500 and 600 °C in air. The samples were heated at a rate of 30 °C/min up to the firing temperature, held at that temperature for 1 h, and then cooled to room temperature inside the furnace. Undoped SnO<sub>2</sub> thin films were utilized for the high-resolution transmission electron microscopy (HRTEM) characterization.

### 2.3. TEM characterization

Focused ion-beam microscopy (FIB) (FIB 200 TEM, FEI Company, Hillsboro, Oregon) milling technique was performed on the undoped SnO<sub>2</sub> thin film for TEM sample preparation. The choice between the doped- and undoped SnO<sub>2</sub> thin films for the TEM sample preparation was as per convenience. The procedure for the TEM sample preparation via FIB milling technique is described in detail elsewhere [36] and was adopted in the present investigation. In short, the FIB-milling procedure involved the sputtering of ~80–100 nm thick Au–Pd layer followed by the deposition of ~1 μm thick Pt-layer over the SnO<sub>2</sub> thin film in order to protect the film from getting destroyed during the FIB-milling operation. HRTEM (FEI-Philips Tecnai F30) was then used to study the structure and the average nanocrystallite size distribution as well as to observe lattice image showing different orientations of nanocrystals within the SnO<sub>2</sub> thin film. Bright field TEM images at 300 kV were taken to observe the lattices. Selected area-electron diffraction (SAED) pattern was collected from the center of the SnO<sub>2</sub> thin film to analyze the crystal structure, which also provided the evidence of the presence of nanocrystals having different orientations within the SnO<sub>2</sub> thin film.

### 2.4. Sensor test

The sensor test set-up has already been described elsewhere [37]. The procedure used for the sensor test is as follows. Four thin film sensors and one bare glass substrate (reference) were mounted on the software designed fiber glass test-board, which incorporated the heater, electrical, and thermocouple connections. During the testing, each sensor was connected in parallel with 10 MΩ resistance using a switcher circuit. The four-probe technique, with a constant-current (100 nA) source, was used to measure the equivalent resistance ( $R_{eq}$ ) in air as well as in the hydrogen-

containing environment. The true resistance values for the thin film sensors in air ( $R_{\text{air}}$ ) and in the hydrogen-containing environment ( $R_{\text{gas}}$ ) were back calculated using the respective measured  $R_{\text{eq}}$  values. The hydrogen gas sensitivity was then determined using the relationship of the form:

$$\text{sensitivity (\%)} = \frac{R_{\text{air}} - R_{\text{gas}}}{R_{\text{gas}}} \times 100, \quad (1)$$

The sensor test was first conducted at room temperature (25 °C). At the beginning of the test, pure nitrogen gas was blown into the test chamber, housing the test board, at 760 Torr for 24 h to remove the water vapor and any residual hydrogen. The pressure inside the test chamber was reduced to 15–50 Torr and was maintained for the next 24 h to stabilize the sensor resistance, which was followed by the measurement of  $R_{\text{air}}$  values. A mixture of nitrogen and hydrogen gas was then admitted into the chamber (chamber volume  $\approx$  50 l). The amount of hydrogen within this mixture was gradually increased in steps within the range of 100 ppm–4 vol.% using mass flow controllers, where the upper amount has been set as an explosive limit by NASA for the space shuttle application.  $R_{\text{gas}}$  values were measured after every 50 s till the sensor resistances dropped sufficiently in the hydrogen-containing environment. At the end of the test, the air at 760 Torr was blown into the chamber to recover the initial resonance of the sensors. Similar test procedure was repeated at 50 °C. Typical cyclic test, consisting of one cycle, was conducted for 3–4 vol.% hydrogen at room temperature (25 °C). During this test, sufficient time was given for the stabilization of the sensor resistances in the hydrogen-containing environment before blowing the air at 760 Torr.

### 3. Results

The TEM and HRTEM images of nanocrystalline undoped  $\text{SnO}_2$  thin film, sol-gel dip-coated on the glass substrate, are presented in Figs. 1(a) and (b), respectively. In Fig. 1(a), the  $\text{SnO}_2$  thin film is observed to be continuous, dense, and without any cracks. The film thickness is observed to vary within the range of  $\sim$ 100–150 nm. The Au-Pd and Pt layers observed in Fig. 1(a) originate from the FIB-milling procedure. Further, in Fig. 1(b), even at very high magnification, the nanocrystalline- $\text{SnO}_2$  thin film appears to be highly dense and without any porosity. Under the given processing conditions, the average  $\text{SnO}_2$  nanocrystallite size of  $\sim$ 6–7 nm is observed from Fig. 1(b).

The variation in the hydrogen gas sensitivity of  $\text{SnO}_2$ -6.5 mol%  $\text{In}_2\text{O}_3$  thin film sensors as a function of amount of hydrogen in higher concentration range (0–4 vol.%), at 25 and 50 °C, is presented in Figs. 2(a) and (b), respectively. At 25 °C (Fig. 2(a)) the hydrogen gas sensitivity of  $\text{SnO}_2$ -6.5 mol%  $\text{In}_2\text{O}_3$  thin film sensors, is observed to follow the parabolic relationship with increasing amount of hydrogen and lies within the range of 15–50%. The thin film sensors calcined at 600 °C, with and

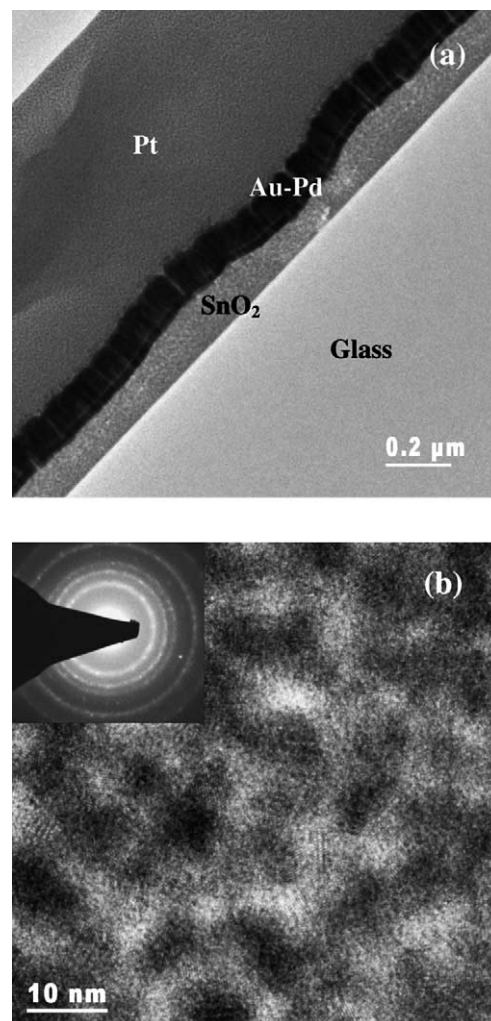


Fig. 1. TEM (a) and HRTEM (b) images of sol-gel dip-coated nanocrystalline undoped  $\text{SnO}_2$  thin film obtained from the FIB-cut TEM sample.

without Pt-sputtering, exhibit higher hydrogen sensitivity than the those calcined at 500 °C. For the calcination treatment at 600 °C, higher hydrogen gas sensitivity is observed for non-Pt-sputtered thin film relative to Pt-sputtered thin film. This trend is, however, reversed for the calcination treatment at 500 °C.

At 50 °C (Fig. 2(b)) the hydrogen gas sensitivity of non-Pt-sputtered  $\text{SnO}_2$ -6.5 mol%  $\text{In}_2\text{O}_3$  thin film sensors, calcined at 500 and 600 °C, is very low. However, Pt-sputtered thin film sensors exhibit very high hydrogen gas sensitivity. The hydrogen gas sensitivity of Pt-sputtered thin film sensor calcined at 500 °C, is higher than that calcined at 600 °C. The hydrogen gas sensitivity of Pt-sputtered thin film sensors lies within the range of 20,000–70,000% for the amount of hydrogen within the concentration range of 1–4 vol.%. The hydrogen gas sensitivity of Pt-sputtered thin film sensors is observed increase with increasing amount of hydrogen. The hydrogen gas sensitivity, however, reaches the respective maximum value at 1 vol.% hydrogen and then remains almost constant with further increase in the amount

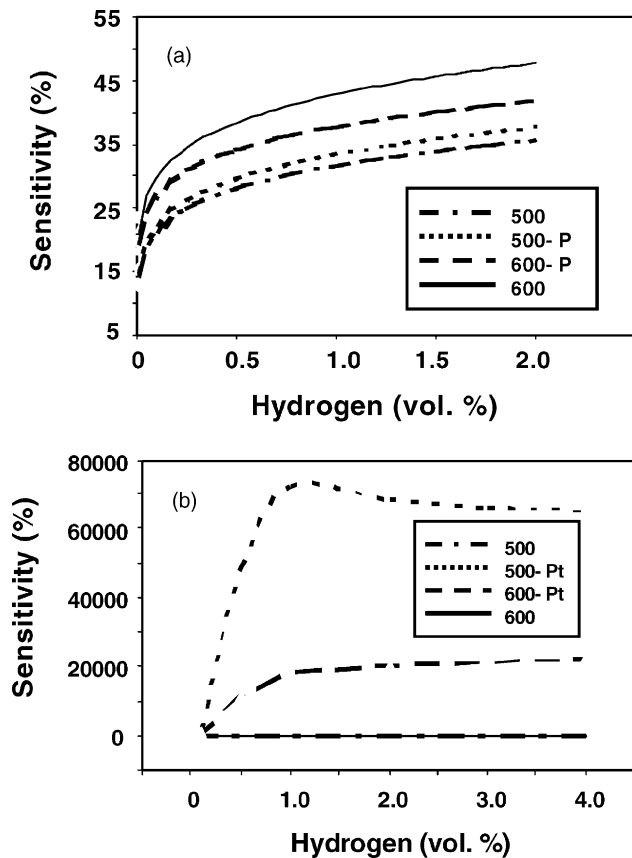


Fig. 2. The variation in the hydrogen gas sensitivity of nanocrystalline 6.5 mol%  $\text{In}_2\text{O}_3$ -doped  $\text{SnO}_2$  thin film sensor as a function of hydrogen concentration in the higher range ( $>5000$  ppm) at  $25^\circ\text{C}$  (a) and  $50^\circ\text{C}$  (b).

of hydrogen. Comparison between Figs. 2(a) and (b) shows that increase in the operating temperature from  $25$  to  $50^\circ\text{C}$  results in a drastic enhancement in the hydrogen gas sensitivity of Pt-sputtered  $\text{SnO}_2$ -6.5 mol%  $\text{In}_2\text{O}_3$  thin film sensors.

The variation in the hydrogen gas sensitivity of  $\text{SnO}_2$ -6.5 mol%  $\text{In}_2\text{O}_3$  thin film sensors as a function of amount of hydrogen, within the lower concentration range (100–1000 ppm), at  $25^\circ\text{C}$  and  $50^\circ\text{C}$ , is presented in Figs. 3(a) and (b), respectively. In Fig. 3(a), the hydrogen gas sensitivity is observed to increase with increasing amount of hydrogen and lies within the range of 12–32%. At both the operating temperatures, the overall trend in the variation in the hydrogen gas sensitivity as a function of amount of hydrogen, appears to be almost similar to that observed in the higher concentration range (0–4 vol.%) (Fig. 2).

At  $50^\circ\text{C}$  (Fig. 3(b)) the Pt-sputtered  $\text{SnO}_2$ -6.5 mol%  $\text{In}_2\text{O}_3$  thin film sensors exhibit higher hydrogen gas sensitivity relative to non-Pt-sputtered thin film sensors, the trend which is similar to the one observed in Fig. 2(b). The Pt-sputtered thin film sensors exhibit low hydrogen gas sensitivity for the amount of hydrogen within the concentration range of 100–400 ppm. However, the hydrogen gas sensitivity is observed to increase rapidly as the concentration of

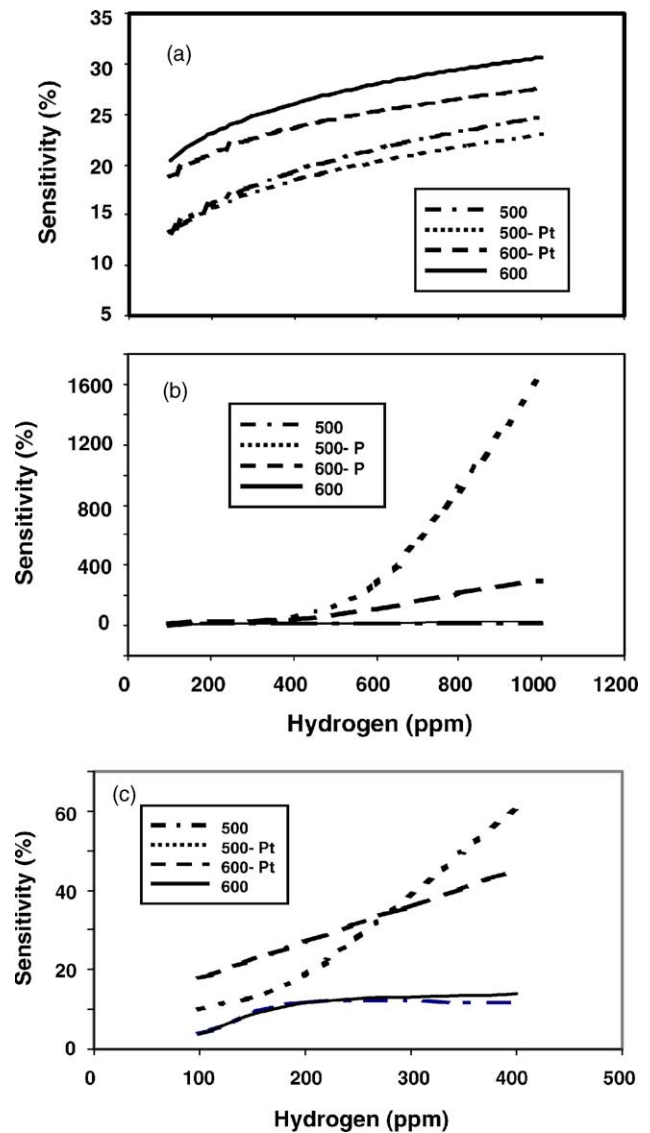


Fig. 3. The variation in the hydrogen gas sensitivity of nanocrystalline 6.5 mol%  $\text{In}_2\text{O}_3$ -doped  $\text{SnO}_2$  thin film sensor as a function of hydrogen concentration in lower range ( $<1000$  ppm) at  $25^\circ\text{C}$  (a) and  $50^\circ\text{C}$  (b). (c) is the enlarged portion of (b) within the hydrogen concentration range of 100–400 ppm.

hydrogen increases within the range of 400–1000 ppm. For 1000 ppm of hydrogen, the maximum hydrogen gas sensitivity of 1600 and 300% is recorded for the Pt-sputtered thin film sensors calcined at 500 and  $600^\circ\text{C}$ , respectively.

As mentioned earlier, in Fig. 3(b), the hydrogen gas sensitivity appears to be very low and independent of amount of hydrogen within the concentration range of 100–400 ppm. Hence, in Fig. 3(c), the enlarged view of the variation in the hydrogen gas sensitivity of  $\text{SnO}_2$ -6.5 mol%  $\text{In}_2\text{O}_3$  thin film sensor as a function of amount of hydrogen, within the concentration range of 100–400 ppm, at  $50^\circ\text{C}$ , is presented. The hydrogen gas sensitivity is not independent of the amount of hydrogen, within the concentration range of 100–400 ppm. On contrary, the hydrogen gas sensitivity is

observed to increase with increasing amount of hydrogen within this concentration range. Initially, for lower amount of hydrogen within this concentration range, Pt-sputtered thin film sensor calcined at 600 °C, exhibit higher hydrogen gas sensitivity than the one calcined at 500 °C. However, the rate of increase in the hydrogen gas sensitivity, with increasing amount of hydrogen, is observed to be larger for the latter. For 400 ppm hydrogen, the maximum hydrogen gas sensitivity of 60 and 45% is recorded for Pt-sputtered thin film sensors calcined at 500 and 600 °C, respectively. On the other hand, the hydrogen gas sensitivity of non-Pt-sputtered thin film sensors, increases marginally with increase in the amount of hydrogen, within the range of 100–200 ppm, and then remains constant at 10% with further increase in the amount of hydrogen.

The variation in the resistance of the SnO<sub>2</sub>–6.5 mol% In<sub>2</sub>O<sub>3</sub> thin film sensors as a function of time, for 3–4 vol.% (explosive limit as set by NASA) hydrogen at 25 °C, is shown in Fig. 4. The cyclic response of non-Pt-sputtered thin film sensors is presented in Fig. 4(a), while that of

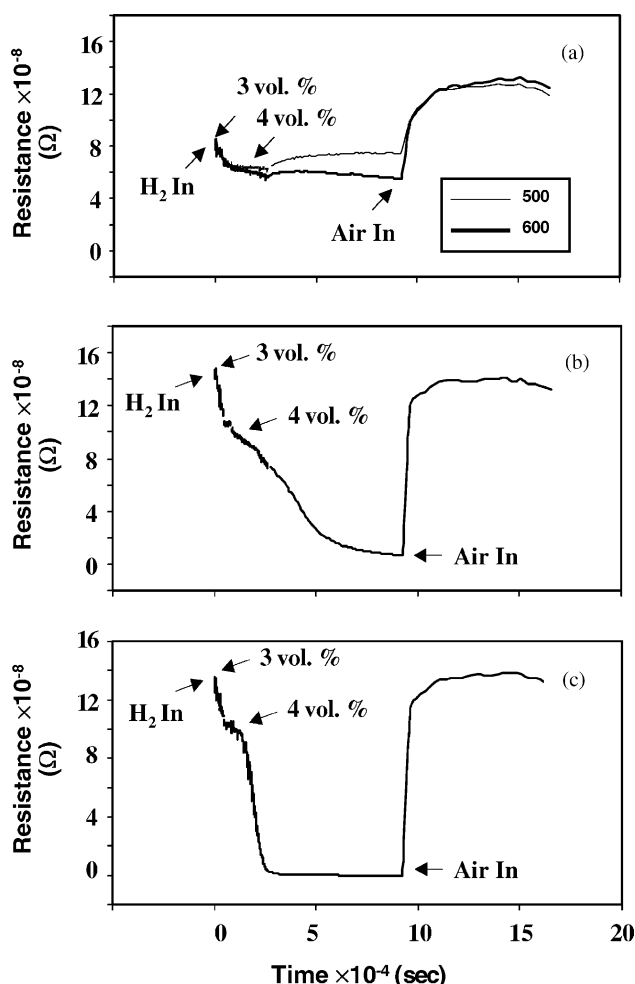


Fig. 4. The response behavior of nanocrystalline 6.5 mol% In<sub>2</sub>O<sub>3</sub>-doped SnO<sub>2</sub> thin film sensor for 3–4 vol.% (explosive limit) hydrogen at 25 °C. (a) corresponds to non-Pt-sputtered thin film sensors and (b–c) correspond to Pt-sputtered thin film sensors calcined at 600 and 500 °C, respectively.

the Pt-sputtered thin film sensors is presented in Fig. 4(b) and (c), respectively. The Pt-sputtered thin film sensors (Fig. 4(b) and (c)) exhibit large decrease in the resistance as compared to the non-Pt-sputtered thin film sensors (Fig. 4(a)). Very high sensitivity values as high as 107,887 and 2083% are observed for the Pt-sputtered thin film sensors calcined at 500 and 600 °C, respectively. Moreover, the Pt-sputtered thin film sensor, calcined at 500 °C (Fig. 4(c)), exhibit faster response relative to the thin film sensor calcined at 600 °C (Fig. 4(b)). The response (90% decrease in the resistance) and the recovery time (85% recovery of the original resistance) are, however, relatively higher at room temperature (Fig. 4(b) and (c)).

#### 4. Discussion

In the present investigation, hydrogen gas is successfully sensed at lower operating temperatures (room temperature (25 °C) and 50 °C) using the nanocrystalline (6–7 nm), 6.5 mol% In<sub>2</sub>O<sub>3</sub>-doped SnO<sub>2</sub> thin (100–150 nm) film sensor. Two different sensing behaviors have been observed at room temperature (25 °C) and 50 °C. Typically, at room temperature (25 °C), although marginal, the gas sensitivity of the sensors calcined at 600 °C (both Pt-sputtered and non-Pt-sputtered thin films) is observed to be higher than the ones calcined at 500 °C (except at very large hydrogen concentration of 4 vol.%). On the other hand, at 50 °C, the gas sensitivity of the Pt-sputtered sensors is higher than the non-Pt-sputtered thin film sensors. Moreover, for the Pt-sputtered sensors, lower calcination temperature (500 °C) is observed to be effective in enhancing the hydrogen gas sensitivity. Hence, overall analysis shows that, at room temperature (25 °C), higher calcination temperature (600 °C), without Pt-sputtering, is more conducive in enhancing the hydrogen sensitivity (except at very high hydrogen concentration of 4 vol.%); while at 50 °C, lower calcination temperature (500 °C), with Pt-sputtering, are the important factors.

There exist several parameters, such as the nanocrystallite size, the film thickness, the amount of film porosity, the calcination and operating temperatures, which simultaneously affect the gas sensitivity of SnO<sub>2</sub> sensor [38]. Hence, we first discuss the role of each individual parameters in enhancing the hydrogen sensitivity based on the literature data and then explain the observed gas sensing behavior of the present In<sub>2</sub>O<sub>3</sub>-doped SnO<sub>2</sub> sensor.

##### 4.1. Characteristics of sol–gel derived nanocrystalline SnO<sub>2</sub> thin film gas sensor (review of literature data)

###### 4.1.1. Role of nanocrystallite size

Using the literature data [22,29,39–43], it has been demonstrated [38] that, below a critical size of 10 nm, the gas sensitivity of the sol–gel derived nanocrystalline SnO<sub>2</sub> sensor increases drastically with decrease in the nanocrystallite size. However, above this critical size, the gas sensitivity

is almost independent of the nanocrystallite size. According to the existing model [35], the mechanism, which controls the resistance of the nanocrystalline SnO<sub>2</sub> thin film, changes as the nanocrystallite size ( $D$ ) changes relative to its space-charge layer thickness ( $L$ ). When  $D \gg 2L$ ,  $D > 2L$ , and  $D \leq 2L$ , the resistance of the thin film is primarily governed by the ‘grain-boundary-control’, the ‘neck-control’ and the ‘grain-control’ mechanisms, respectively. The gas sensitivity of the nanocrystalline SnO<sub>2</sub> thin film is enhanced only when the film resistance is controlled by the latter two mechanisms, especially by the ‘grain-control’ mechanism. For the SnO<sub>2</sub> thin film and sintered powders, the space-charge layer thickness has been calculated to be 3 nm at 250 °C [44,45]. As a result, the transducer function of the nanocrystalline SnO<sub>2</sub> thin film is activated below 10 nm crystallite size, thus enhancing its gas sensitivity.

Although not explained by the earlier model [35], the small SnO<sub>2</sub> nanocrystallite size (<10 nm), also activates the receptor function of the semiconductor oxide, which in turn aids in enhancing the gas sensitivity [46]. Very low activation energy (9 kJ/mol) for the grain growth has been calculated for SnO<sub>2</sub> nanocrystallites within the size range of 3–20 nm [46]. Above this size range (20–300 nm), the activation energy for the grain growth is calculated to be 91 kJ/mol. Very low activation energy for the grain growth, calculated for the size range of 3–20 nm, has been attributed to the possible generation of an excess oxygen-ion vacancy concentration within the SnO<sub>2</sub> lattice. The excess lattice oxygen-ion vacancy concentration, below a critical nanocrystallite size, has also been predicted for other ceramic oxides [47,48]. In the case of nanocrystalline SnO<sub>2</sub>, this excess lattice oxygen-ion vacancy concentration can lead to an increased adsorption of oxygen ions (O<sub>2</sub><sup>-</sup> and O<sup>-</sup> ions) on the surface, which in turn can enhance the receptor function of the semiconductor thin film gas sensor. Using Monte-Carlo computer simulation technique [49], it has been shown that, the excess lattice oxygen-ion vacancy concentration is responsible for the surface-adsorbed oxygen ions (O<sub>2</sub><sup>-</sup> and O<sup>-</sup> ions) in the large amount. Hence, it appears that, the enhanced gas sensitivity of the nanocrystalline SnO<sub>2</sub> thin film sensor, below a critical size of 10 nm, is due to its enhanced receptor as well as transducer functions below this critical size. In the present investigation, under the given processing conditions, SnO<sub>2</sub>-nanocrystallites of size 6–7 nm are obtained via sol-gel dip-coating process, which are conducive for sensing the hydrogen gas at lower operating temperatures.

#### 4.1.2. Role of film thickness

It appears from the reported data [29,39,40,50,51] that the gas sensitivity of nanocrystalline SnO<sub>2</sub> thin film increases with decreasing film thickness [38]. However, below a critical film thickness of ~110 nm, the gas sensitivity decreases with further decrease in the film thickness.

The increase in the gas sensitivity with decrease in the film thickness can be explained on the basis of the model proposed by Sakai et al. [11]. According to this model, the

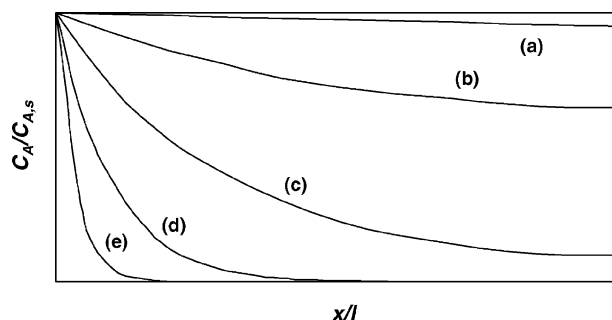


Fig. 5. Generalized gas concentration profiles within SnO<sub>2</sub> thin film, having straight channel structure, with increasing function of  $l(k/D_K)^{1/2}$  (a–e).

concentration of the gas molecules ( $C_A$ ) at a distance of ‘ $x$ ’ from the surface, within a porous SnO<sub>2</sub> thin film having thickness ‘ $l$ ’, is given by:

$$C_A = C_{A,S} \frac{\sinh[x(k/D_K)^{1/2}] + \sinh[(2l-x)(k/D_K)^{1/2}]}{\sinh[2l(k/D_K)^{1/2}]}, \quad (2)$$

where,  $C_{A,S}$  is the surface-concentration of the gas molecules,  $k$  the rate constant of the surface reaction, and  $D_K$  the Knudsen diffusion coefficient. Fig. 5 is a generalized profile obtained from Eq. (2), which shows the relation between  $C_A/C_{A,S}$  and  $x/l$  with  $l(k/D_K)^{1/2}$  as a parameter. It is clearly observed that, for a fixed value of  $(k/D_K)^{1/2}$ , flat profile is exhibited by thin films (low  $l(k/D_K)^{1/2}$ ). On the other hand, for thick films (high  $l(k/D_K)^{1/2}$ ), the concentration of the gas molecules within the film is restricted to the near-surface region. As the gas molecules are likely to diffuse throughout the film thickness, thin films exhibit larger gas sensitivity relative to thick films. As a result, the gas sensitivity tends to increase with decreasing film thickness.

However, the above model fails to explain the reverse trend observed below the film thickness of ~110 nm. It is to be noted that, the amount of porosity within the nanocrystalline SnO<sub>2</sub> thin films is shown to decrease drastically below the film thickness of 70–200 nm [11,52]. Very compact films exhibit lower surface areas and reduced Knudsen diffusion coefficient. As a result, they offer reduced number of active sites for the oxidation reactions with the reducing gases, and hence, would reduce the gas sensitivity with decreasing film thickness below this critical thickness range. In the present investigation, the nanocrystalline SnO<sub>2</sub> film thickness of 100–150 nm, obtained via sol-gel dip-coating process, is comparable with the optimum film thickness corresponding to the maximum gas sensitivity reported in the literature and is conducive for sensing the hydrogen at lower operating temperatures.

#### 4.1.3. Role of film porosity

The gas sensitivity is observed to increase with increasing amount of film porosity [12,38,52]. It is demonstrated that [38] the gas sensitivity of the nanocrystalline SnO<sub>2</sub>

semiconductor thin film sensor increases from 100 to 900% with increase in the amount of film porosity from 32 to 65%. The gas sensitivity is also predicted [11] to increase with increase in the pore diameter as a result of an enhanced knudsen diffusion coefficient ( $D_K$ ), which for straight round pores within the thin film, is given by [11]:

$$D_K = 9700 \times r \left( \frac{T}{M} \right)^{1/2}, \quad (3)$$

where,  $r$  is the pore radius,  $T$  the absolute temperature (K), and  $M$  the molecular weight of the gas. For a given film thickness, large pore radius increases  $D_K$ , and hence, would favor the flat gas concentration profile (Fig. 5) thus enhancing the gas sensitivity. In the present investigation, although the sol-gel dip-coated thin films are observed to be non-porous, Fig. 1, the hydrogen is successfully sensed at lower operating temperatures (room temperature (25 °C) and 50 °C). Hence, it appears that, the hydrogen gas sensitivity of the present sensor, at lower operating temperatures (room temperature (25 °C) and 50 °C), can be further enhanced by synthesizing porous thin films.

#### 4.1.4. Role of calcination temperature

The combined literature data [22,29,39–43,50–52] shows that, the maximum gas sensitivity is observed for the calcination temperature of 450 °C, below and above which, the gas sensitivity decreases [38]. The calcination treatment is generally applied to crystallize the as-deposited amorphous thin films, and to control the film density and the nanocrystallite size. The lower calcination temperature generally results in incomplete crystallization of the amorphous thin film while the higher calcination temperature results in the grain growth. As a result, the gas sensitivity may be reduced due to the calcination treatment at very low and very high temperatures. Due to the optimum balance between the amount of crystallization and the grain growth, the maximum sensitivity value is generally reported at the intermediate calcination temperature of 450 °C. In the present investigation, the SnO<sub>2</sub>–6.5 mol% In<sub>2</sub>O<sub>3</sub> thin film is calcined at 500 and 600 °C, which are above but close to the optimum calcination temperature related to the maximum gas sensitivity.

#### 4.1.5. Role of operating temperature

Using the literature data [22,29,39–43,50–52], it is further demonstrated that [38], the maximum gas sensitivity of the nanocrystalline SnO<sub>2</sub> thin film sensor is observed at the operating temperature range of 320–350 °C, below and above which the gas sensitivity decreases. Within the lower operating temperature range of 100–320 °C, the desorption of water and adsorption of the oxygen ions (O<sub>2</sub><sup>−</sup> and O<sup>−</sup> ions) dominates [12], which increases the film resistance as well as the gas sensitivity due to increased number of active surface sites (O<sub>2</sub><sup>−</sup> and O<sup>−</sup> ions) for the chemical reaction with the reducing gases. Moreover, the reduced activation energy for the chemical reaction between the

reducing gases and the surface-adsorbed oxygen ions (O<sub>2</sub><sup>−</sup> and O<sup>−</sup> ions) favors higher gas sensitivity with increasing operating temperature. On the other hand, in the higher operating temperature range, 350–500 °C, desorption of the surface-adsorbed oxygen ions dominates. As a result, the number of active surface sites (O<sub>2</sub><sup>−</sup> and O<sup>−</sup> ions), for the chemical reaction with the reducing gases, are reduced within the higher operating temperature range. This reduces the film resistance and the gas sensitivity with increasing operating temperature within this range [12,29]. In addition to this, an instability in the microstructure (grain growth) may also have its own effect in reducing the gas sensitivity within the higher operating temperature range (350–500 °C). In the present investigation, hydrogen is sensed at very lower operating temperatures (room temperature (25 °C) and 50 °C), where the literature data is still lacking. At such lower operating temperatures, the activation energy for the chemical reaction between the hydrogen gas and surface-adsorbed oxygen ions (O<sub>2</sub><sup>−</sup> and O<sup>−</sup> ions) would be higher, the number of active surface sites (O<sub>2</sub><sup>−</sup> and O<sup>−</sup> ions) would be lower, but stable nanocrystallite size could be maintained for long period of time. As explained in the next section, the doped-In<sup>3+</sup> cations and the small nanocrystallite size (6–7 nm) are effective in increasing the number of active surface sites (O<sub>2</sub><sup>−</sup> and O<sup>−</sup> ions), thus enabling the present sensor to sense hydrogen at lower operating temperatures.

Thus, the overall analysis of the gas sensing characteristics of the sol-gel derived nanocrystalline SnO<sub>2</sub> thin film sensor, based on the literature data shows that, the maximum gas sensitivity is reported for the following optimum values of the processing and the thin film parameters: (i) nanocrystallite size—<10 nm; (ii) film thickness—110 nm; (iii) amount of film porosity—65%; (iv) calcination temperature—450 °C; (v) operating temperature—320–350 °C.

#### 4.2. Sensing hydrogen at lower operating temperatures (room temperature (25–50 °C))

In the present investigation, under the given sol-gel dip-coating conditions, SnO<sub>2</sub> thin film with nanocrystallite size (6–7 nm) and film thickness (100–150 nm), which are close to the optimum values, is synthesized. However, the undoped SnO<sub>2</sub> thin film could not sense hydrogen below 1 vol.% at room temperature (25 °C) [37]. Hence, in the present investigation, the SnO<sub>2</sub> thin film is doped with In<sup>3+</sup> cations and the resulting film could successfully sense hydrogen at lower operating temperatures (room temperature (25 °C) and 50 °C) at ppm level. This type of trivalent doping generates excess lattice oxygen-ion vacancy concentration to maintain the charge balance, which has two distinct effects. First, it leads to an increased surface adsorption of oxygen ions (O<sub>2</sub><sup>−</sup> and O<sup>−</sup> ions), which enhances the receptor function of the sensor; and secondly, it increases the space-charge layer thickness, which enhances the transducer function of the sensor. It is also noted that the excess

lattice oxygen-ion vacancy concentration may be generated by very small SnO<sub>2</sub> nanocrystallite size (6–7 nm). Moreover, the small nanocrystallite size (6–7 nm) itself is conducive for controlling film resistance via the ‘grain-control’ mechanism. Hence, the small nanocrystallite size is also responsible for enhancing the receptor and the transducer functions of the present sensor.

Hence, the successful sensing of hydrogen at lower operating temperatures (room temperature (25 °C) and 50 °C) at ppm level is attributed to the doped-In<sup>3+</sup> cations, small nanocrystallite size, and small film thickness, which effectively enhanced the receptor and the transducer functions of the present thin film sensor.

It is further noted that, at 50 °C, the Pt-sputtered nanocrystalline thin film sensor calcined at lower temperature (500 °C) exhibits maximum hydrogen gas sensitivity than the one calcined at higher temperature (600 °C). Typically, for 1000 ppm and 2 vol.% hydrogen, maximum sensitivity values of 1600 and 70,000% are respectively noted for the Pt-sputtered sensor calcined at 500 °C. The thin film sensor calcined at 500 °C possibly exhibits smaller nanocrystallite size than the one calcined at 600 °C. As a result, the maximum hydrogen gas sensitivity is observed for the sensor calcined at 500 °C. Moreover, at 50 °C, the Pt-sputtered thin film sensors are observed to exhibit enhanced hydrogen gas sensitivity than the non-Pt-sputtered sensors. This clearly suggests that the Pt-nanoparticles play an important role of a catalyst for sensing hydrogen at 50 °C. Further, it is observed that, at 50 °C, the hydrogen gas sensitivity reaches a saturation value at 1 vol.% hydrogen. This is attributed to the possible consumption of all active surface sites (O<sup>-</sup> and O<sup>2-</sup> ions) by 1 vol.% hydrogen as a result of which the hydrogen sensitivity does not increase with increasing amount of hydrogen above 1 vol.%.

The sensor behavior observed in the present investigation at 50 °C is consistent with the sensor behavior reported in the literature at higher operating temperatures. In contrast to this, at room temperature (25 °C), neither the effect of Pt nor the effect of nanocrystallite size (lower calcination temperature) nor the saturation of hydrogen sensitivity is observed. Typically, for 1000 ppm and 2 vol.% hydrogen maximum sensitivity values of 32% and 50% are respectively noted for the non-Pt-sputtered sensor calcined at 600 °C. No definite explanation can be put forward for the abnormal sensor behavior at room temperature (25 °C) observed during the continuous test (where, the amount of hydrogen is increased in steps). However, the cyclic test conducted at room temperature (25 °C) for 3–4 vol.% hydrogen, does show the effect of Pt and the effect of nanocrystallite size (calcination temperature) in enhancing the hydrogen sensitivity and response kinetics. Typically, for 4 vol.% hydrogen, maximum sensitivity value of 107,887% is noted for the Pt-sputtered sensor calcined at 500 °C. Thus, the room temperature (25 °C) hydrogen sensing at ppm level, using the nanocrystalline In<sub>2</sub>O<sub>3</sub>-doped SnO<sub>2</sub> thin film sensor, is successfully demonstrated in the present investigation;

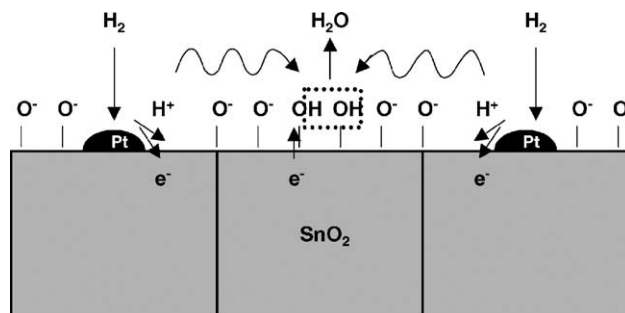
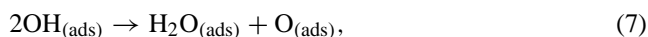
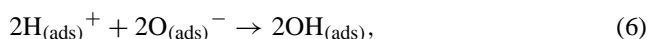
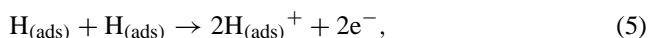


Fig. 6. The mechanism of hydrogen gas sensing for the nanocrystalline Pt-sputtered SnO<sub>2</sub> thin film sensor.

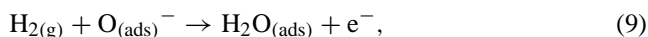
while, enhanced hydrogen sensitivity is demonstrated by marginal increase (by 25 °C) in the operating temperature to 50 °C.

#### 4.3. Mechanism of hydrogen gas sensing

The mechanism of hydrogen gas sensing, at lower operating temperatures, is schematically described in Fig. 6. The hydrogen gas gets decomposed on the surface of Pt-catalyst (present on the sensor surface) to nascent hydrogen atoms, which loose electrons to the conduction band of semiconductor oxide. The generated protons get associated with the surface-adsorbed oxygen ions and hop from one oxygen ion to another. Two adjacent OH groups condense and eliminate H<sub>2</sub>O. In the process, net one electron is injected into the conduction band of doped SnO<sub>2</sub> reducing its resistance. The chemical reactions involved during the hydrogen sensing are summarized below:



The net reaction is:



It appears that, the large concentration of surface-adsorbed oxygen ions (O<sup>-</sup> ions) would favor the forward reaction presented in Eq. (9), thus enhancing the hydrogen sensitivity. In the present investigation, large concentration of surface-adsorbed oxygen ions (O<sup>-</sup> ions) is achieved via doped-In<sup>3+</sup> cations and small nanocrystallite size. Secondly, it is also noted that, at lower operating temperatures (room temperature (25 °C) and 50 °C), the eliminated H<sub>2</sub>O (product) would be in the form of water molecule, and hence, may remain adsorbed on the sensor surface. The presence of surface contamination (H<sub>2</sub>O molecules) possibly reduces the hydrogen gas sensitivity and the reaction kinetics at lower operating temperatures since their presence may hamper the

forward reaction presented in Eq. (9). The abnormal sensor behavior observed at room temperature (25 °C) may possibly be related to the surface contamination by H<sub>2</sub>O molecules. It is hypothesized that higher calcination temperature (600 °C) may generate more thermal stresses resulting in more cracks within the thin film sensor. In the presence of surface contamination (H<sub>2</sub>O molecules), these cracks may play an important role in enhancing the hydrogen sensitivity for the sensor calcined at higher calcination temperature (600 °C). Further detailed investigation is, however, needed to confirm this hypothesis.

## 5. Conclusions

- (1) Hydrogen gas, within the concentration range of 100 ppm–4 vol.%, is successfully sensed at lower operating temperatures (room temperature (25 °C) and 50 °C) using the sol–gel dip-coated nanocrystalline (6–7 nm) 6.5 mol% In<sub>2</sub>O<sub>3</sub>-doped SnO<sub>2</sub> semiconductor thin (100–150 nm) film sensor.
- (2) Typically, for 1000 ppm of hydrogen, the maximum sensitivity values of 32 and 1600% are observed at room temperature (25 °C) and 50 °C, respectively, for the non-Pt-sputtered sensor calcined at 600 °C and Pt-sputtered sensor calcined at 500 °C, respectively. For 2 vol.% hydrogen, the maximum sensitivity values of 50 and 70,000% are recorded at room temperature (25 °C) and 50 °C, respectively, for the non-Pt-sputtered sensor calcined at 600 °C and Pt-sputtered sensor calcined at 500 °C, respectively. At room temperature (25 °C), for 4 vol.% hydrogen (explosive limit as set by NASA), the maximum hydrogen sensitivity values of 107,887 and 2083% are observed (via cyclic test) for the Pt-sputtered sensors calcined at 500 and 600 °C, respectively.
- (3) The lower calcination temperature (that is, smaller nanocrystallite size) and the presence of Pt-catalyst are observed to enhance the hydrogen sensitivity at 50 °C. The hydrogen sensitivity and the response kinetics are also observed to be enhanced at room temperature (25 °C), due to smaller nanocrystallite size and the presence of Pt-catalyst, for the cyclic test conducted for 3–4 vol.% hydrogen. However, the abnormal behavior observed during the continuous-test (where, the amount of hydrogen is increased in steps) cannot be explained at this stage, but may be related to the combined effect of surface contamination by H<sub>2</sub>O molecules and the presence of thin film cracks generated by the thermal stresses.

## Acknowledgements

The authors thank UCF, Florida Space Grant Consortium, FSEC (NASA Glenn), NASA, National Science Foundation (NSF EEC-0136710) for funding the sensor and the nano-technology research.

## References

- [1] W.-C. Liu, H.-J. Pan, H.-I. Chen, K.-W. Lin, C.-K. Wang, Comparative hydrogen-sensing study of Pd/GaS and Pd/InP metal-oxide–semiconductor Schottky diodes, *Jpn. J. Appl. Phys. Part 1* 40 (2001) 6254–6259.
- [2] P. Tobiska, O. Hugon, A. Trouillet, H. Gangnaire, An integrated optic hydrogen sensor based on SPR on palladium, *Sens. Actuators B* 74 (2001) 168–172.
- [3] F. Favier, E.C. Walter, M.P. Zach, T. Benter, R.M. Penner, Hydrogen sensors and switches from electrodeposited palladium mesowire arrays, *Science* 293 (2001) 2227–2231.
- [4] R. Bouchet, S. Rosini, G. Vitter, E. Siebert, Solid-state hydrogen sensor based on acid-doped polybenzimidazole, *Sens. Actuators B* 76 (2001) 610–616.
- [5] W. Shin, K. Imai, N. Izu, N. Murayama, Thermoelectric thick-film hydrogen gas sensor operating at room temperature, *Jpn. J. Appl. Phys. Part 2: Lett.* 40 (2001) L1232–L1234.
- [6] W.P. Jakubik, M.W. Urbanczyk, S. Kochowski, J. Bodzenta, Bilayer structure for hydrogen detection in a surface acoustic wave sensor system, *Sens. Actuators B* 82 (2002) 265–271.
- [7] D.R. Baselt, B. Fruhberger, E. Klaassen, S. Cemalovic, C.L. Britton Jr., S.V. Patel, T.E. Mlsna, D. McCorkle, B. Warmack, Design and performance of a microcantilever-based hydrogen sensor, *Sens. Actuators B* 88 (2003) 120–131.
- [8] Y. Zhang, S. Asahina, S. Yoshihara, T. Shirakashi, Fabrication and characterization of diamond quartz crystal microbalance electrode, *J. Electrochem. Soc.* 149 (2002) H179–H182.
- [9] I. Simon, M. Arndt, Thermal and gas-sensing properties of a micro-machined thermal conductivity sensor for the detection of hydrogen in automotive applications, *Sens. Actuators A* 97–98 (2002) 104–108.
- [10] Y. Shimizu, Y. Nakamura, M. Egashira, Effects of diffusivity of hydrogen and oxygen through pores of thick film SnO<sub>2</sub>-based sensors on their sensing properties, *Sens. Actuators B* 13 (1993) 128–131.
- [11] G. Sakai, N.S. Baik, N. Miura, N. Yamazoe, Gas sensing properties of tin oxide thin films fabricated from hydrothermally treated nanoparticles: dependence of CO and H<sub>2</sub> response on film thickness, *Sens. Actuators B* 77 (2001) 116–121.
- [12] N.S. Baik, G. Sakai, N. Miura, N. Yamazoe, Hydrothermally treated sol solution of tin oxide for thin-film gas sensor, *Sens. Actuators B* 63 (2000) 74–79.
- [13] W.K. Choi, S.K. Song, J.S. Cho, Y.S. Yoon, D. Choi, H.-J. Jung, S.K. Koh, H<sub>2</sub> gas-sensing characteristics of SnO<sub>x</sub> sensors fabricated by a reactive ion-assisted deposition with/without an activator layer, *Sens. Actuators B* 40 (1997) 21–27.
- [14] S.-K. Song, J.-S. Cho, W.-K. Choi, H.-J. Jung, D. Choi, J.-Y. Lee, H.-K. Baik, S.-K. Koh, Structure and gas-sensing characteristics of undoped tin oxide thin films fabricated by ion-assisted deposition, *Sens. Actuators B* 46 (1998) 42–49.
- [15] K.H. Cha, H.C. Park, K.H. Kim, Effect of palladium doping and film thickness on the H<sub>2</sub>-gas sensing characteristics of SnO<sub>2</sub>, *Sens. Actuators B* 21 (1994) 91–96.
- [16] G. Sberveglieri, G. Faglia, S. Groppelli, P. Nelli, Methods for the preparation of NO, NO<sub>2</sub> and H<sub>2</sub> sensors based on tin oxide thin films, grown by means of the r.f. magnetron sputtering technique, *Sens. Actuators B* 8 (1992) 79–88.
- [17] V.V. Malyshev, A.A. Vasiliev, A.V. Eryshkin, E.A. Kolytyn, Y.I. Shubin, A.I. Buturlin, V.A. Zaikin, G.B. Chakhunashvili, Gas sensitivity of SnO<sub>2</sub> and ZnO thin-film resistive sensors to hydrocarbons, carbon monoxide and hydrogen, *Sens. Actuators B* 10 (1992) 11–14.
- [18] V.N. Mishra, R.P. Agarwal, Thick-film hydrogen sensor, *Sens. Actuators B* 21 (1994) 209–212.
- [19] H.-J. Michel, H. Lieste, K.D. Schierbaum, J. Halbritter, Adsorbates and their effects on gas sensing properties of sputtered SnO<sub>2</sub> films, *Appl. Surf. Sci.* 126 (1998) 57–64.

- [20] G.S. Devi, S.K. Masthan, M. Shakuntala, V. Rao, Correlation between structural properties and gas sensing characteristics of SnO<sub>2</sub> based gas sensors, *J. Mater. Sci.: Mater. Electron.* 10 (1999) 545–549.
- [21] A. Katsuki, K. Fukui, H<sub>2</sub> selective gas sensor based on SnO<sub>2</sub>, *Sens. Actuators B* 52 (1998) 30–37.
- [22] V. Jayaraman, K.I. Gnanasekar, E. Prabhu, T. Gnanasekaran, G. Periaswami, A low temperature H<sub>2</sub> sensor based on intermediate hydroxy tin oxide, *Sens. Actuators B* 55 (1999) 147–153.
- [23] V.A. Choudhary, I.S. Mulla, K. Vijayamohan, Comparative studies of doped and surface modified tin oxide towards hydrogen sensing: synergistic effects of Pd and Ru, *Sens. Actuators B* 50 (1998) 45–51.
- [24] V.A. Choudhary, I.S. Mulla, K. Vijayamohan, Selective hydrogen sensing properties of surface functionalized tin oxide, *Sens. Actuators B* 55 (1999) 154–160.
- [25] Y.-D. Wang, C.-L. Ma, X.-H. Wu, X.-D. Sun, H.-D. Li, Electrical and gas-sensing properties of mesostructured tin oxide-based H<sub>2</sub> sensor, *Sens. Actuators B* 85 (2002) 270–276.
- [26] J. Zhang, K. Colbow, Surface silver clusters as oxidation catalysts on semiconductor gas sensors, *Sens. Actuators B* 40 (1997) 47–52.
- [27] A. Cabot, A. Dieguez, A.R. Rodriguez, J.R. Morante, N. Barsan, Influence of the catalytic introduction procedure on the nano-SnO<sub>2</sub> gas sensor performances: where and how stay the catalytic atoms? *Sens. Actuators B* 79 (2001) 98–106.
- [28] S.C. Tsang, C.D.A. Bulpitt, C.H. Mitchell, A.J. Ramirez-Cuesta, Some new insights into the sensing mechanism of palladium promoted tin (IV) oxide sensor, *J. Phys. Chem. B* 105 (2001) 5737–5742.
- [29] J.W. Hammond, C.-C. Liu, Silicon based microfabricated tin oxide gas sensor incorporating use of Hall effect measurement, *Sens. Actuators B* 81 (2001) 25–31.
- [30] S. Matsushima, T. Maekawa, J. Tamaki, N. Yamazoe, New methods for supporting palladium on a tin oxide gas sensor, *Sens. Actuators B* 9 (1992) 71–78.
- [31] G.-J. Li, S. Kawi, High-surface-area SnO<sub>2</sub>: a novel semiconductor-oxide gas sensor, *Mater. Lett.* 34 (1998) 99–102.
- [32] F. Lu, Y. Liu, M. Dong, X. Wang, Nanosized tin oxide as the novel material with simultaneous detection towards CO, H<sub>2</sub>, and CH<sub>4</sub>, *Sens. Actuators B* 66 (2000) 225–227.
- [33] S. Seal, S. Shukla, Nanocrystalline SnO gas sensor in view of surface reactions and modifications, *JOM* 54 (2002) 35–38, 60.
- [34] E.R. Leite, I.T. Weber, E. Longo, J.A. Varela, New method to control particle size and particle size distribution of SnO<sub>2</sub> nanoparticles for gas sensor applications, *Adv. Mater.* 12 (2000) 965–968.
- [35] C. Xu, J. Tamaki, N. Miura, N. Yamazoe, Grain size effects on gas sensitivity of porous SnO<sub>2</sub>-based elements, *Sens. Actuators B* 3 (1991) 147–155.
- [36] B.I. Prenitzer, L.A. Giannuzzi, K. Newman, S.R. Brown, R.B. Irwin, T.L. Shoftner, F.A. Stevie, Transmission electron microscope specimen preparation of Zn powders using the focused ion beam lift-out technique, *Mater. Trans. A* 29 (1998) 2399–2406.
- [37] S. Shukla, S. Patil, S.C. Kuiry, S. Seal, Z. Rahman, L. Ludwig, C. Parish, Synthesis and characterization of sol-gel derived nanocrystalline SnO<sub>x</sub> thin film as a hydrogen gas sensor, *Sens. Actuators B*, in press.
- [38] S. Shukla, S. Seal, Sol-gel derived nanocrystalline semiconductor oxide thin film gas sensors, in: H.S. Nalwa (Ed.), *Encyclopedia of Nanoscience and Nanotechnology*, American Scientific Publishers, Stevenson Ranch, CA, 2003, in press.
- [39] Z. Jin, H.-J. Zhou, Z.-L. Jin, R.F. Savinell, C.-C. Liu, Application of nano-crystalline porous tin oxide thin film for CO sensing, *Sens. Actuators B* 52 (1998) 188–194.
- [40] G. De, A. Licciulli, C. Massarao, A. Quirini, R. Rella, P. Siciliano, L. Vasanelli, Sol-gel derived pure and palladium activated tin oxide films for gas-sensing applications, *Sens. Actuators B* 55 (1999) 134–139.
- [41] A. Licciulli, S. Mazzarelli, G. De, P. Siciliano, L. Vasanelli, R. Rella, Os and Pd modified tin oxide films for sensors by the sol gel process, *J. Sol-Gel Sci. Technol.* 21 (2001) 195–201.
- [42] G. Zhang, M. Liu, Effect of particle size and dopant on properties of SnO<sub>2</sub>-based gas sensors, *Sens. Actuators B* 69 (2000) 144–152.
- [43] A. Carbot, J. Arbiol, J.R. Morante, W. Weimar, N. Barsan, W. Gopel, Analysis of the noble metal catalytic additives introduced by impregnation of as obtained SnO<sub>2</sub> sol-gel nanocrystals for gas sensors, *Sens. Actuators B* 70 (2000) 87–100.
- [44] C. Xu, J. Tamaki, N. Miura, N. Yamazoe, Relationship between gas sensitivity and microstructure of porous SnO<sub>2</sub>, *J. Electrochem. Soc. Jpn.* 58 (1990) 1143–1148.
- [45] H. Ogawa, M. Nishikawa, A. Abe, Hall measurement studies and an electrical conduction model of tin oxide ultrafine particle films, *J. Appl. Phys.* 53 (1982) 4448–4455.
- [46] S. Shukla, S. Seal, Room temperature gas sensitivity of nanocrystalline pure tin oxide, *J. Nanosci. Nanotechnol.*, in press.
- [47] S. Shukla, S. Seal, R. Vij, S. Bandyopadhyay, Reduced activation energy for grain growth in nanocrystalline yttria stabilized zirconia, *Nano Lett.* 3 (2003) 397–401.
- [48] X.-D. Zhou, W. Hueber, Size-induced lattice relaxation in CeO<sub>2</sub> nanoparticles, *Appl. Phys. Lett.* 79 (2001) 3512–3534.
- [49] P.D. Skafidas, D.S. Vlachos, J.N. Avaritsiotis, Modelling and simulation of abnormal behavior of thick-film tin oxide gas sensors in CO, *Sens. Actuators B* 21 (1994) 109–121.
- [50] R. Rella, A. Serra, P. Siciliano, L. Vasanelli, G. De, A. Licciulli, Quirini, Tin oxide-based gas sensors prepared by the sol-gel process, *Sens. Actuators B* 44 (1997) 462–467.
- [51] F. Quaranta, R. Rella, P. Siciliano, S. Capone, M. Epifani, L. Vasanelli, A. Licciulli, A. Zocco, A novel gas sensor based on SnO<sub>2</sub>/Os thin film for the detection of methane at low temperature, *Sens. Actuators B* 58 (1999) 350–355.
- [52] S.-S. Park, J.D. Mackenzi, Thickness and microstructure effects on alcohol sensing of tin oxide thin films, *Thin Solid Films* 274 (1996) 154–159.